Kondo hybridization and quantum criticality in β-$YbAlB_4$ by laser ARPES

Cédric Bareille,[1,*] Shintaro Suzuki,[1] Mitsuhiro Nakayama,[1] Kenta Kuroda,[1] Andriy H. Nevidomskyy,[2] Yosuke Matsumoto,[3] Satoru Nakatsuji,[1,4] Takeshi Kondo,[1] and Shik Shin[1]

[1]*ISSP, University of Tokyo, Kashiwa 277-8581, Japan*

[2]*Department of Physics and Astronomy & Center for Quantum Materials, Rice University, Houston, Texas 77005, USA*

[3]*Max Planck Institute for Solid State Research, Heisenbergstrasse 1, Stuttgart 70569, Germany*

[4]*CREST, Japan Science and Technology Agency (JST), 4-1-8 Honcho Kawaguchi, Saitama 332-0012, Japan*

(Received 16 June 2017; revised manuscript received 29 October 2017; published 10 January 2018)

We report an angle-resolved photoemission (ARPES) study of β-$YbAlB_4$, which is known to harbor unconventional quantum criticality (QC) without any tuning. We directly observe a quasiparticle peak (QP) emerging from hybridization, characterized by a binding energy and an onset of coherence both at about 4 meV. This value conforms with a previously observed reduced Kondo scale at about 40 K. Consistency with an earlier study of carriers in β-$YbAlB_4$ via the Hall effect strongly suggests that this QP is responsible for the QC in β-$YbAlB_4$. A comparison with the sister polymorph α-$YbAlB_4$, which is not quantum critical at ambient pressure, further supports this result. Indeed, within the limitation of our instrumental resolution, our ARPES measurements do not show tangible sign of hybridization in this locally isomorphic system, while the conduction band we observe is essentially the same as in β-$YbAlB_4$. We therefore claim that we identified by ARPES the carriers responsible for the QC in β-$YbAlB_4$. The observed dispersion and the underlying hybridization of this QP are discussed in the context of existing theoretical models.

DOI: 10.1103/PhysRevB.97.045112

I. INTRODUCTION

The formation of a nonmagnetic Kondo-singlet ground state commonly provides a description of heavy Fermi liquid (FL) in intermetallic rare-earth compounds. It emerges below the Kondo temperature T_K from the screening of the local moments of f orbitals by conduction electrons, which accompanies the onset of coherence of a quasiparticle (QP) peak binding at $k_B T_K$: the Kondo resonance peak [1]. When external parameters are accurately tuned, numerous heavy-fermion systems deviate from this normal FL. In the conventional scenario, spin-density-wave instabilities induce such non-FL behavior by driving the system to the critical regime of a magnetic quantum transition [2]. In β-$YbAlB_4$, quantum criticality (QC) has been observed below about 4 K at zero magnetic field and ambient pressure [3], away from any magnetic order [4]. Therefore, it cannot be cast in this usual picture of magnetic instability. Moreover, it shows an unexpected (T/B) scaling [3,5] and unusual critical exponents [6], which challenge theoretical descriptions. Diverse works [7–12] attempt to model this unconventional QC, without any possible consensus. Although the FL behavior is recovered with a moderate magnetic field, its description and formation in term of Kondo screening are still poorly understood. Indeed, despite a large Kondo scale $T_K \approx 250$ K, incoherent skew scattering is observed down to $T_{coh} \approx 40$ K [13], and magnetic moments are still present as low as $T^* \approx 8$ K [5]. Kondo lattice behavior finally sets in only below T^*. Advanced analysis of Hall effect measurements shed some light by the identification of two different components of carriers with distinct Kondo scales [13], which we call carriers a and carriers b for convenience. Carriers a govern the longitudinal transport with T_K as the Kondo scale and a relatively high carrier density n_a^{Hall}, while carriers b have a low carrier density n_b^{Hall} with electronlike character and gain coherence below a second Kondo scale at T_{coh}. The conclusion from Hall effect measurements further identifies carriers b as responsible for both Kondo lattice and QC behaviors below T^* [13]. Nevertheless, the details about the emergence of these carriers and about the underlying Kondo physics are still lacking.

In the present article, we take advantage of the apparent location of the QC at zero magnetic field, without tuning of any control parameter [3], to directly probe QP in β-$YbAlB_4$ by high-resolution laser ARPES. To highlight any relation between microscopic observations and the QC, we also perform ARPES measurements on the sister compound α-$YbAlB_4$, whose structure is sketched alongside that of β-$YbAlB_4$ in Fig. 1(a). This locally isomorphic compound exhibits very similar behaviors and temperature scales, however, unlike β-$YbAlB_4$, it does not display QC, developing instead a heavy Fermi liquid [14]. Moreover, it has been shown that the magnetization in β-$YbAlB_4$ can be separated into two components: the QC component and a heavy Fermi-liquid component similar to that in α-$YbAlB_4$ [5]. Thus, α-$YbAlB_4$ is a perfect control system to study the unconventional criticality in β-$YbAlB_4$.

Our measurements reveal the hybridization between the crystal-field split heavy Yb f-electron bands and a light conduction band in β-$YbAlB_4$. The resulting electronlike QP has a binding energy and an onset of coherence at about 4 meV, consistent with carriers b highlighted by Hall measurements as responsible for the QC. By contrast, we find almost no or very weak hybridization in the sister α-phase, while the

*bareille@issp.u-tokyo.ac.jp

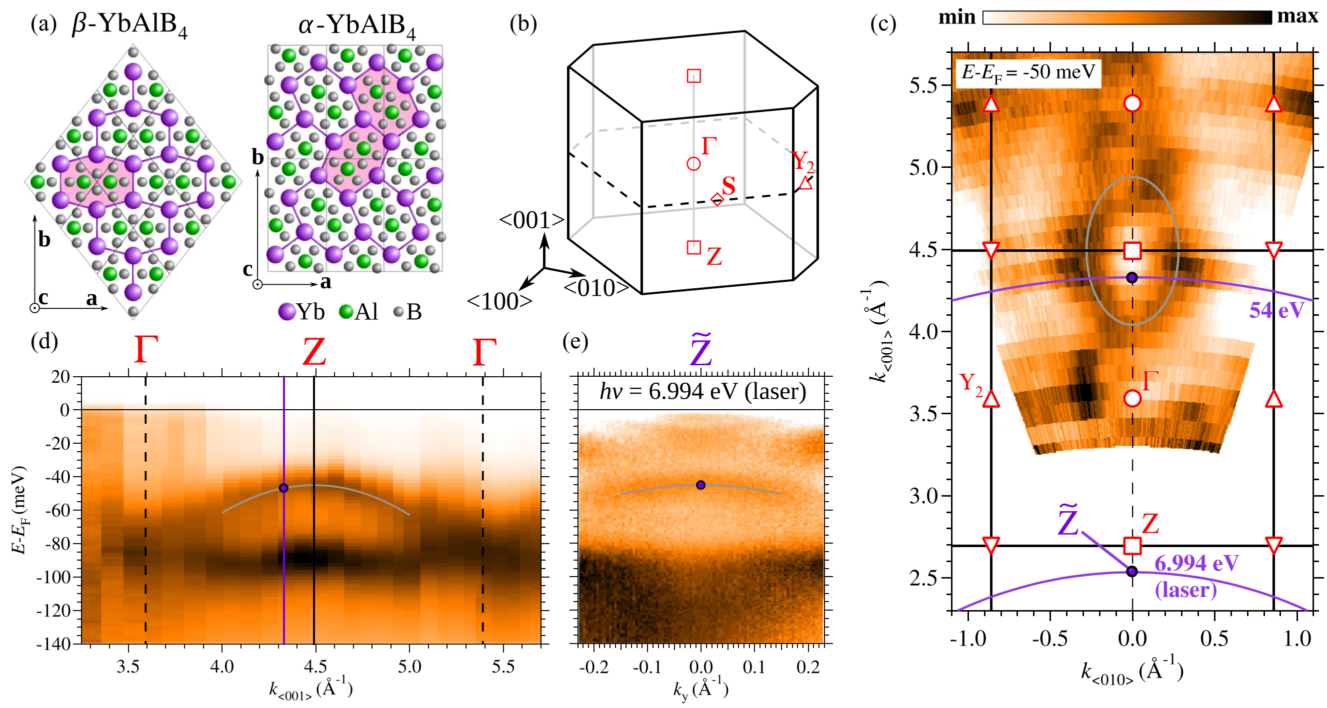

FIG. 1. (a) Representation from the c axis of the crystal structure of β-$YbAlB_4$ (left) and α-$YbAlB_4$ (right). (b) Brillouin zone of β-$YbAlB_4$. (c) Mapping in the (100) plane, 50 meV below E_F. Full black lines are the edges of the BZ. Purple circles show the position reached with a light of $h\nu = 6.994$ and 54 eV. (d) Dispersion at normal emission, i.e., along the $\langle 001 \rangle$ direction. (e) Laser-ARPES spectra on β-$YbAlB_4$; $h\nu = 6.994$ eV.

dispersion of the conduction band is very similar between the two phases. Our results strongly suggest the importance of the Kondo hybridization for the microscopic mechanism behind the QC in β-$YbAlB_4$.

II. METHODS

High-quality single crystals were grown by using the Al-flux method as described in the literature [15]. The excess Al flux was etched by a water solution of sodium hydroxide. All ARPES measurements were performed with a SES R4000 analyzer in a chamber shielded from magnetic field by mu-metal. Clean surfaces were obtained by cleaving crystals along the (a,b) plane in ultrahigh vacuum (below 5×10^{-11} Torr). Measurements in the (100) plane were carried out at the 1-cubed end-station at Helmholtz-Zentrum Berlin by tuning the photon energy from 24 to 120 eV, thanks to the synchrotron radiation of the BESSY-II facility. The temperature was about 1 K, and the overall resolution was about 10 meV. Measurements in the (001) plane for both β and α phases were realized with a 6.994 eV laser at the ISSP, at a temperature of 5 K, with an overall resolution of about 3 meV. Data from β-$YbAlB_4$ were measured with circular polarized light, while data from α-$YbAlB_4$ were measured with linear horizontal polarized light. Nevertheless, as Fig. S1 of the Supplemental Material shows [16], measurements with linear horizontal polarized light give similar results to those with circular polarized light. Thus, this difference does not affect our observations. Treatments by 2D curvature of some spectra of this work are performed following the method described in Ref. [17].

III. RESULTS

The β-$YbAlB_4$ crystal has an orthorhombic structure [15]; Fig. 1(b) schematizes the corresponding Brillouin zone (BZ). Samples were cleaved along the (a,b) plane to perform photoemission. Figure 1(c) shows the edges of the BZ overlaid on a mapping in the (100) plane, 50 meV below the Fermi level, while the dispersion along the normal emission Γ-Z line is displayed in Fig. 1(d). Conversion into momentum space was made in the frame of the nearly-free-electron final-state approximation [18]. The inner potential was determined to be $V_0 \approx 22$ eV thanks to the point-group symmetry and periodicity, with, as a main indication, a holelike band centered on the Z point, depicted by the gray parabola in panel (d) and the gray ellipse in panel (c). Also visible in panel (d) is a nearly flat band bounded at about 100 meV below E_F—it is a part of the Yb^{2+} $|J = 7/2\rangle$ multiplet, which has been previously observed by x-ray photoemission spectroscopy [19]. Complete investigation and discussion over the full three-dimensional BZ will be part of a future work. Here, we will focus instead on the results from laser-ARPES, which, while being more restricted in **k** space, offers very high resolution and intensity.

Given the laser photon energy $h\nu = 6.994$ eV, the available BZ cut is depicted by the lower purple circle in Fig. 1(c), which crosses the Γ-Z line less than 0.2 Å^{-1} below the Z point, named $\tilde{Z}$ for convenience. Measurements with photon energy $h\nu = 54$ eV reach an equivalent position along the Γ-Z line [see the higher purple circle in Fig. 1(c)]. The dispersive holelike band with the top bound at about -45 meV, as well as the flat band at about -90 meV, were observed using the light source both with photon energy $h\nu = 54$ eV [see panels (c) and (d)] as well

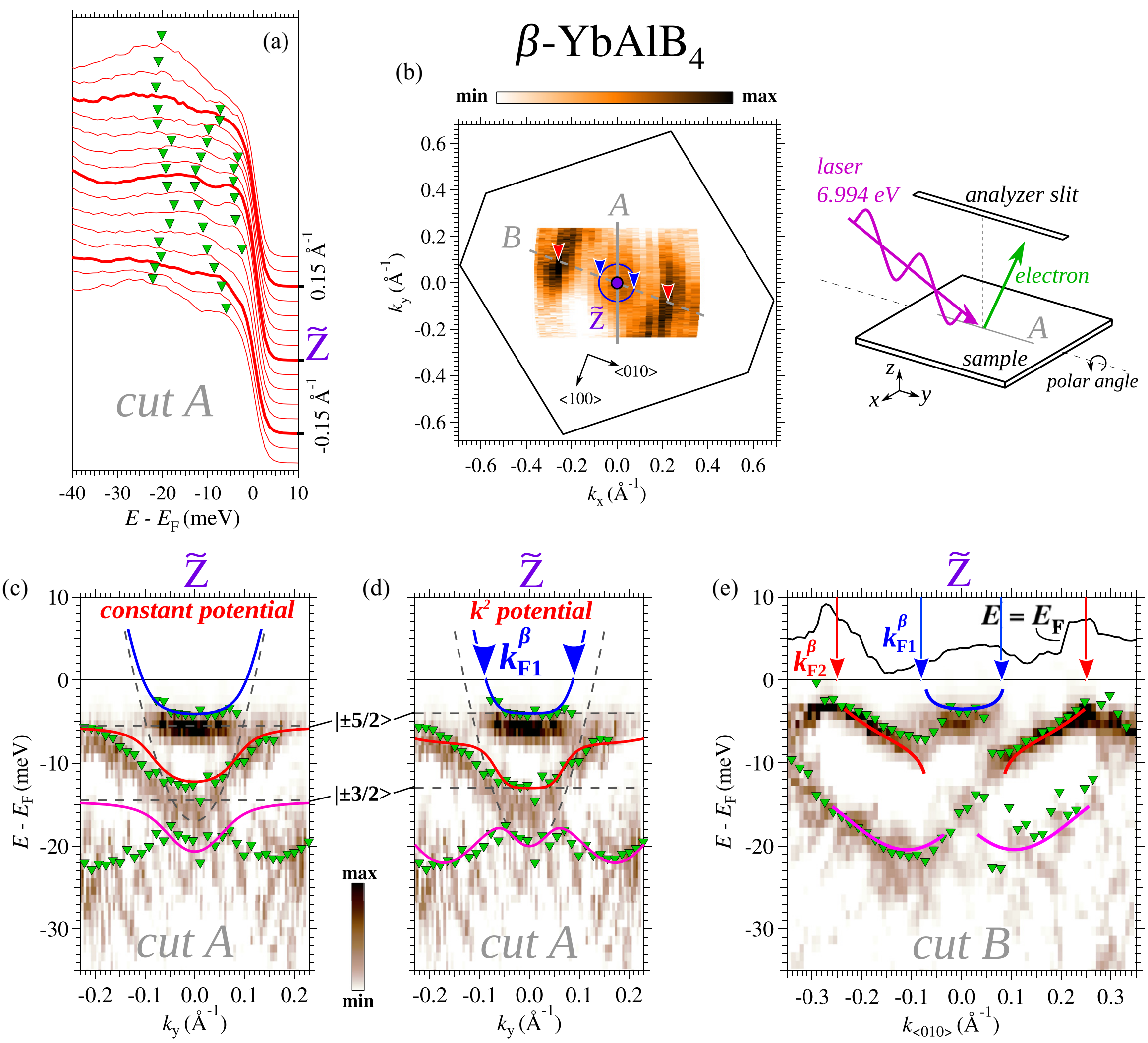

FIG. 2. Laser-ARPES on β-YbAlB$_4$. (a) Stack of EDCs next to $\tilde{Z}$, along the full gray line A in panel (b). Green markers are peak position from EDCs, fitted by Voigt with a quadratic background and cut by a Fermi-Dirac step. Detailed fitting for $k_y = -0.15$, 0, and 0.15 Å^{-1} are illustrated with Fig. S2 of the Supplemental Material [16]. (b) Fermi-surface mapping performed by tuning the polar angle. Sketch on the right illustrates the geometry of the measurements; the analyzer slit was oriented along the line A. The blue circle shows the little electronlike Fermi sheet, while the two red arrows show an outer Fermi sheet. Black lines are edges of the BZ. (c) Curvature of the ARPES spectra measured along the slit of the analyzer [full gray line in panel (b)]. Green markers are peak position as of panel (a). The blue, red, and pink lines are the results of the modeling based on the constant hybridization of the original bands (represented by dashed black lines). (d) Same as (c) with a **k**-dependent nodal potential. See the Supplemental Material for the raw data (Fig. S3) and details of the hybridization models [16]. (e) Curvature of the cut along the ⟨010⟩ direction [dashed gray line B in panel (b)]. Green markers are peak position from EDC fit. Full blue, red, and pink lines are guides to the eye. See Fig. S3 of the Supplemental Material for the raw data [16].

as with the laser in panel (e), thus providing a calibration of our laser-ARPES. In what follows, we focus on the bands above $E > -40$ meV, which are observable thanks to laser-ARPES, and we compare them to our measurements on α-YbAlB$_4$.

We investigate the vicinity of E_F with the stack of energy distribution curves (EDCs), Fig. 2(a), extracted along k_y, i.e., along the analyzer slit, with $k_x = 0$ [full gray line A in Fig. 2(b)]. We observe three dispersions; they can be modeled by a light electronlike band with $m^* \approx 3m_e$ and the band bottom of ≈20 meV below E_F, which hybridizes and forms anticrossings with two flat bands, a first one around −4 meV and a second one around −13 meV [thin dashed lines in Figs. 2(c) and 2(d)]. These two flat bands, separated by 9 meV, are consistent with the crystal electric field of about 80 K, extracted from fitting the magnetic susceptibility [20]. From this fitting and local symmetry considerations detailed in Ref. [20], the two flat bands can then be identified as the ground state $J_z = \pm 5/2\,(|\pm 5/2\rangle)$, at −4 meV, and the first crystal-field excited state, dominated by $J_z = \pm 3/2\,(|\pm 3/2\rangle)$, at −13 meV, of the $J = 7/2$ Yb multiplet. In Fig. 2(c), solid lines are the results of fitting to the hybridization model with a constant hybridization function $V \approx 4$ meV. The first anticrossing at −5 meV is nicely fitted, and forms an electronlike QP band [blue line in Fig. 2(c)] bound at about 4 meV below E_F. This energy scale, one order of magnitude smaller than $T_K \approx 250$ K, is consistent with the expectation from previous experimental observations [13,14] of a reduced Kondo scale at $T_{coh} \approx 40$ K (≈3.4 meV).

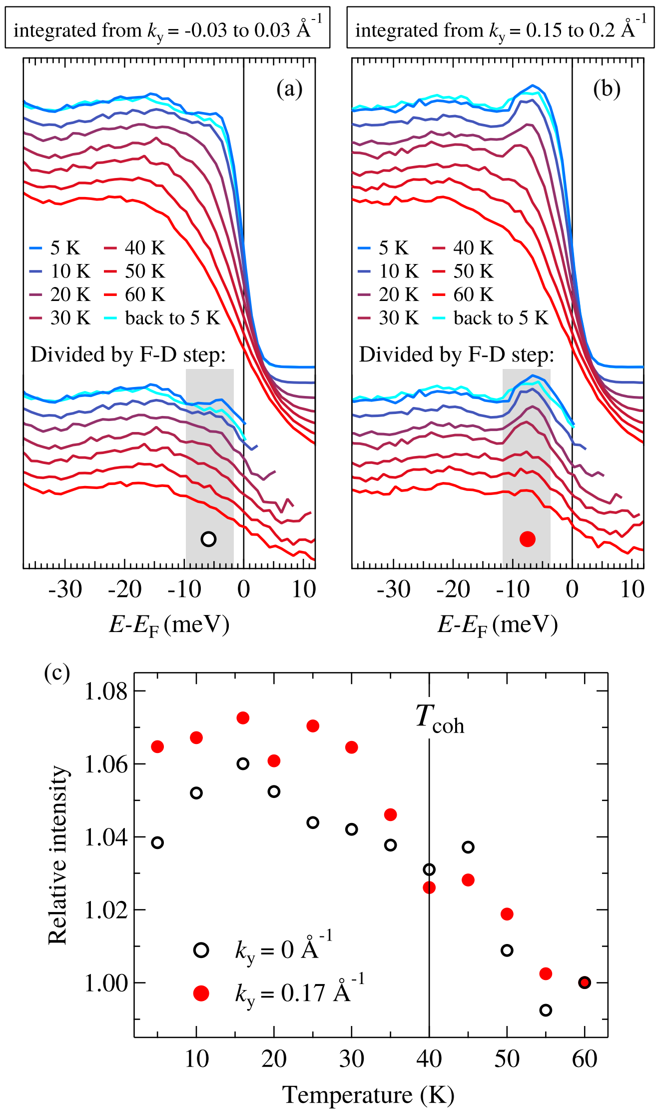

FIG. 3. Temperature dependence on β-YbAlB$_4$. (a) EDCs at $k_y = 0$ Å^{-1} from $T = 5$ to 60 K. (b) EDCs at $k_y = 0.17$ Å^{-1} from $T = 5$ to 60 K. [The peak's intensity difference with EDC in Fig. 2(a) is due to a slightly different orientation along the slit, as temperature dependence was performed on a different sample—see Fig. S1 of the Supplemental Material for the corresponding color scale [16]]. (c) Intensity, relative to the value at 60 K, of the inner (outer) peak from EDCs divided by the Fermi-Dirac step and integrated along the shade area of panel (a) [(b)].

The temperature dependence of EDCs in Fig. 3 confirms the relation between the QP peak and T_{coh}. Panels (a) and (b) show EDCs from 5 to 60 K at the inner ($k_y = 0$ Å^{-1}) and outer ($k_y = 0.17$ Å^{-1}) sides of the anticrossing, respectively. The same EDCs divided by the Fermi-Dirac step are displayed at the bottom of these two panels. For both, the QP peak slowly disappears as the temperature goes up. It is clearer on the outer EDCs where the peak intensity suddenly drops from 30 to 40 K. The peak is totally restored by cooling back down (light blue EDC), showing that our observations are not due to surface degradation. For both inner and outer peaks, the intensity integrated along the shaded area [see panels (a) and (b), respectively] of EDCs divided by the Fermi-Dirac step is displayed against the temperature in panel (c), relative to the value at 60 K. Both peaks slowly drop when temperature crosses T_{coh}. It is worthwhile to emphasize that, to our knowledge, it is the first direct and fully resolved observation by ARPES of a Kondo-like hybridization with unified binding energy, onset of coherence, and Kondo scale. While a similar observation has been reported on YbRh$_2$Si$_2$, both the QP peak and the hybridization gap were not fully resolved [21].

Nevertheless, here the second anticrossing at $E \approx -15$ meV is badly reproduced by the constant hybridization model [pink line in Fig. 2(c)]. By taking **k**-dependent hybridization proposed theoretically [8,20], we obtain a more satisfying fit, as shown by the pink line in Fig. 2(d). The significance of **k**-dependent hybridization is developed in the discussion section. The fitting parameters of both models are detailed in the Supplemental Material [16]. Finally, the hybridization with the $|\pm 5/2\rangle$ level at about -4 meV results in the small electronlike QP peak [blue line in panels (c) and (d) of Fig. 2], which crosses the Fermi level at $k_{F1}^{\beta} \approx 0.09$ Å^{-1} and has a mass of about $3m_e$ at E_F. It forms quite an isotropic Fermi sheet, as can be seen via the in-plane mapping at E_F in Fig. 2(b) (blue circle). The size, mass, and isotropy of this small pocket are compatible with the observations by quantum oscillations on β-YbAlB$_4$ [22].

It should be noted that, along the $\langle 010\rangle$ direction, the $|\pm 5/2\rangle$ level crosses E_F at about $k_{F2}^{\beta} \approx 0.25$ Å^{-1}. This second Fermi momentum is exhibited by red arrows on the Fermi mapping, Fig. 2(b), as well as on the cut along the $\langle 010\rangle$ direction, Fig. 2(e). Blue, red, and pink full lines are guides to the eye for the same dispersions as Fig. 2(d). The observation of a second Fermi momentum implies an overlapping of the blue and red hybridized bands in Fig. 2(e). To account for it, we need to introduce a small dispersion to the $|\pm 5/2\rangle$ level in our model, corresponding to a mass $m_f^* \approx 70m_e$ in the $\langle 010\rangle$ direction. This very large mass makes it difficult to be observed by quantum oscillations.

Carrier density can be estimated at the $T = 0$ limit assuming spherical Fermi sheets by $n = k_F^3/3\pi^2$ [23]. Before hybridization, the little conduction band has a density of $n_c^{\mathrm{ARPES}} \approx 7.4 \times 10^{25}$ m^{-3}. It is of the same order as the value estimated from Hall measurements [13] of carriers b at $T = 140$ K (i.e., above the integration of the f electron to the Fermi surface): $n_b^{\mathrm{Hall}}(T = 140\text{ K}) \approx 16 \times 10^{25}$ m^{-3}. Below T_{coh}, the carrier density could not be accurately extracted from the Hall measurements. Yet, estimation of the density of the two Fermi sheets from our measurements (i.e., including f electrons), $n^{\mathrm{ARPES}} \approx 55 \times 10^{25}$ m^{-3}, is still one order of magnitude smaller than the density of carriers a identified as the main contribution to the transport by Hall effect measurements, estimated at 50 K to $n_a^{\mathrm{Hall}}(T = 50\text{ K}) \approx 416 \times 10^{25}$ m^{-3}. Therefore, carriers of β-YbAlB$_4$ observed here, thanks to the high resolution of laser-ARPES, match carriers b identified as being responsible for both Kondo lattice and QC behaviors below T^* by Hall effect measurements. Specifically, they are of electronlike character, gain coherence below T_{coh}, and have low carrier density. From this evidence, we argue that the observed Fermi sheets and the underlying Kondo hybridization

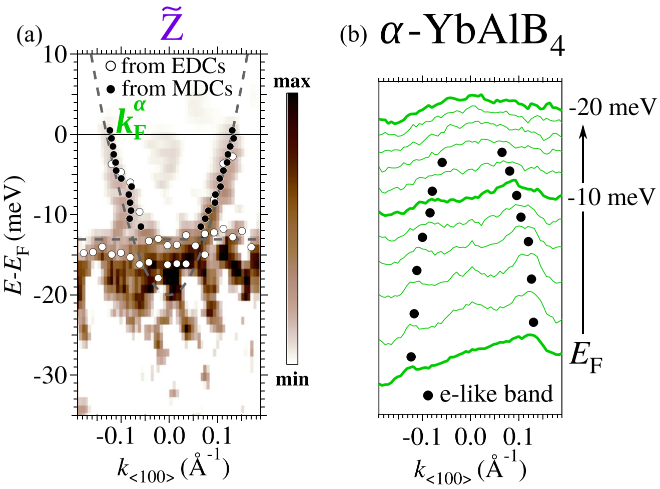

FIG. 4. Laser-ARPES on α-YbAlB$_4$. (a) Curvature of the spectra along the ⟨100⟩ direction. Open and full circles are peak positions, extracted, respectively, from EDCs and MDCs. See Fig. S3 of the Supplemental Material for the raw data [16]. (b) MDC stack of previous panel. Black markers are peak positions for the electronlike band. They were obtained by fitting MDCs by Voigts with a constant background.

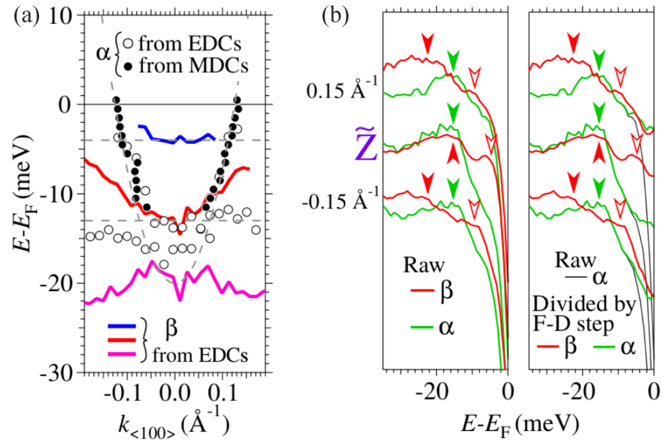

FIG. 5. (a) MDC and EDC fits (open and full markers) from α-YbAlB$_4$ compared to EDC fit on β-YbAlB$_4$ (blue, red, and pink lines). The broken black lines denote the unhybridized electronlike conduction band and Yb $4f$ flat bands from the same model as in Fig. 2. (b) EDCs at $k = 0$; ± 0.15 Å^{-1} from β-YbAlB$_4$ (red) and α-YbAlB$_4$ (green). In the left panel is the raw, while the right panel shows the EDCs divided by the effective Fermi-Dirac step. Open arrows indicate the $|\pm 5/2\rangle$ level, while full arrows indicate the $|\pm 3/2\rangle$ level.

are closely related to both Kondo lattice and QC behaviors below T^*.

To verify our claim, we now look at the electronic structure of the sister compound α-YbAlB$_4$ in the vicinity of E_F. Figure 4(a) displays the laser-ARPES curvature spectra along the ⟨100⟩ direction, where mainly two features are visible: an almost flat band and a light electronlike band dispersing all the way up to E_F. The former is revealed by fitting the peaks in the EDCs (open circles) at about -13 meV below E_F. The dispersive electronlike band is better seen by fitting the peaks from the momentum distribution curves (MDCs) [full circles in Figs. 4(a) and 4(b)] down to -12 meV; the two peaks are difficult to distinguish at higher binding energies. The peaks are directly visible on the stack of MDCs, Fig. 4(b). This light dispersion crosses E_F at $k_F^\alpha \approx 0.13$ Å^{-1}.

In Fig. 5(a), we compare the two aforementioned bands with the ones observed in β-YbAlB$_4$. Intriguingly, they are identical to the dispersive electronlike band and the flat $|\pm 3/2\rangle$ band derived from the **k**-dependent hybridization model used for β-YbAlB$_4$, copied onto panel (a) with dashed lines. On the other hand, the $|\pm 5/2\rangle$ level is seemingly not observed in α-YbAlB$_4$. A peak is visible at $k = 0$, however it is very limited in momentum space and may correspond to a different conduction band. We directly compare the EDCs from β- and α-YbAlB$_4$ in Fig. 5(b), in red and green lines, respectively. Red open arrows show the $|\pm 5/2\rangle$ level as a peak on the β-YbAlB$_4$ EDCs. On α-YbAlB$_4$, only shoulders are visible. When divided by the Fermi-Dirac step, these shoulders disappear and no peak is left, thus indicating the absence of the $|\pm 5/2\rangle$ level in our data on α-YbAlB$_4$. On the other hand, one would expect the crystal-field splitting to be very similar between these two locally isomorphic phases, and the absence of the $|\pm 5/2\rangle$ level in our data could be a result of a bad sample surface quality, which may especially affect the conclusions so close to E_F. What can be said with certainty, however, is that we do not observe any sign of hybridization between either of the flat Yb $4f$ levels and the conduction electron bands in α-YbAlB$_4$, within our instrumental resolution of ∼3 meV. Indeed, the light electronlike band disperses straight through the -4 meV energy to cut through E_F, while no gap is visible at about -13 meV where one would expect the second anticrossing with the Yb $|\pm 3/2\rangle$ level. This is evidenced by the EDCs in Fig. 5(b): on α-YbAlB$_4$, the $|\pm 3/2\rangle$ level (full green arrows) is at the same position on both $k = 0$ and $k = \pm 0.15$ Å^{-1}, in clear contrast with EDCs on β-YbAlB$_4$. We conclude that the manifestation of the Kondo hybridization in the one-particle spectral function (see Ref. [18]) is much less pronounced in α-YbAlB$_4$ compared to the β-phase, although within the experimental resolution of our laser-ARPES measurements, we cannot exclude manifestations of the hybridization smaller than about ∼3 meV in the α-phase.

IV. DISCUSSION

The absence of a tangible sign of Kondo hybridization in our ARPES data on α-YbAlB$_4$, in contrast to β-YbAlB$_4$, further supports the idea that the hybridization and emerging QP peak play a crucial role in the unconventional quantum criticality observed in the latter compound. Moreover, our analysis shows that the heavy dispersions of β-YbAlB$_4$ are best fitted with a **k**-dependent hybridization function, as put forward by the theory of the critical nodal metal [8]. The key feature of this latter model is that the Kondo hybridization vanishes at the Γ point quadratically in the in-plane momentum (k_x, k_y), stemming from the $|\pm 5/2\rangle$ nature of the f-level. It implies the formation of a nodal line along the c axis, which causes the non-FL behavior in β-YbAlB$_4$ [8]. It is important to note, however, that for this model to explain the observed T/B scaling in

β-YbAlB$_4$, the renormalized position $\tilde{E}_f$ of the ground-state $|\pm5/2\rangle$ doublet must be pinned at the Fermi level. It is therefore difficult to unequivocally corroborate the theoretical model, in its original form, based on our ARPES data. It follows from our ARPES analysis that this doublet actually crosses the Fermi level at the wave vector $k_{F2}^{\beta} \approx 0.25\,\text{Å}^{-1}$ and has an intrinsic bandwidth, characterized by a heavy quasiparticle mass $m_f^* \sim 70m_e$. Clearly, this situation is more complex than in the nodal metal theory of Ref. [8], where the $|\pm5/2\rangle$ doublet was assumed to be perfectly flat, in other words the Yb-Yb electron hopping was neglected. In this situation, it could be possible for a portion of the nodal line to be bound at the Fermi level. Since our present observations already support the **k**-dependent hybridization, investigating the dispersion of the $|\pm5/2\rangle$ doublet along the c axis would be desirable.

We note that the observation of the second Fermi momenta k_{F2}^{β} may also be consistent with the model of deconfinement of the f electrons [24], whose application to β-YbAlB$_4$ has been proposed by Hackl and Thomale [10]. In this model, k_{F2}^{β} hosts the critical fluctuations, while carriers at k_{F1}^{β}, labeled "cold," exhibit a FL behavior. Naively, this is compatible with the similar observation of the Fermi momenta k_F^{α} in the FL of α-YbAlB$_4$. Nevertheless, we did not observe any direct sign of such deconfinement in our data; from the ARPES point of view, measurements at lower temperature are necessary to follow the coherence of the $|\pm5/2\rangle$ and to settle this question. In fact, previous electrical and thermal transport measurements [25] discard this scenario by highlighting a discrepancy with the expectation advanced by Hackl and Thomale of a characteristic maximum in the Wiedemann-Franz ratio [10].

Finally, we note that the band structure observed in the present ARPES measurement is consistent with the theory of electron-spin resonance (ESR) in β-YbAlB$_4$ by Ramires *et al.* [26]. Indeed, in addition to the unconventional QC, β-YbAlB$_4$ shows a singular ESR signal, characterized by hyperfine satellites at low temperature, and by the constancy of the ESR signal intensity [27]. The work of Ramires *et al.* reproduces first the hyperfine satellites by including Yb atoms with nonzero nuclear spin into the Kondo screening, and then the constancy of the signal intensity by a crystal electric field comparable to the Kondo hybridization strength [26]. The band structure we observe in ARPES, with the hybridization of about 4 meV of the same order as the crystal electric field ~9 meV, directly confirms the theoretical assumption in Ref. [26]. Additionally, the absence of tangible sign of the Kondo-like hybridization within the experimental resolution of our ARPES measurements of α-YbAlB$_4$, along with the absence of hyperfine satellites in its ESR signal [28], tends to reinforce this model.

V. CONCLUSIONS

In conclusion, we report an ARPES study of both β- and α-YbAlB$_4$, with the key observation of a Kondo-like hybridization between the crystal-field split Yb f levels and an electronlike conduction band in β-YbAlB$_4$. The crystal-field splitting inferred from our ARPES data has a magnitude of ~9 meV, in good agreement with previous estimation [20]. Based on this agreement, we are able to use the theoretical arguments to identify the low-lying heavy band at -4 meV below E_F as the ground-state $|J_z = \pm5/2\rangle$ doublet, and the band at -13 meV as the first excited crystal-field state, dominated by $|J_z = \pm3/2\rangle$ of the Yb $J = 7/2$ multiplet.

The observed hybridization gives rise to a small electronlike QP pocket whose size and effective mass are consistent with quantum oscillations measurements [22], together with a heavier Fermi sheet as the hybridized bands overlap in energy. Importantly, this QP exhibits a binding energy and an onset of coherence which both conform with the earlier indications of a reduced Kondo coherence temperature $T_{coh} \approx 40$ K [13,14]. Thus, as evidenced by the Hall effect measurements, it is indeed these Fermi sheets that are responsible for both Kondo lattice and QC behaviors below T^* [13].

Measurements of α-YbAlB$_4$ further support our conclusion. Indeed, in α-YbAlB$_4$, we similarly observe the electronlike conduction band and the flat band at -13 meV below E_F, which we also identify as the $|\pm3/2\rangle$ state. However, where β-YbAlB$_4$ shows two anticrossings of Yb $4f$ levels with the dispersive conduction band, the bands in the α phase do not show, within our resolution, any apparent sign of hybridization. This dichotomy strongly suggests that this hybridization plays a crucial role in the unconventional quantum criticality in β-YbAlB$_4$, whereas α-YbAlB$_4$ is not critical at ambient conditions.

While our observations cannot sharply infer the microscopic mechanism behind the non-Fermi-liquid behavior in β-YbAlB$_4$, they provide an important insight for future experimental and theoretical investigations. As we already mentioned, further ARPES measurements at lower temperature, and in wider regions of the Brillouin zone, will have the potential to shed more light on this intriguing quantum critical behavior.

ACKNOWLEDGMENTS

We thank S. Burdin, S. Watanabe, and D. Malterre for helpful discussions. We thank P. Zhang for sharing his procedure to perform 2D curvature. We thank D. Evtushinsky and E. Rienks for their precious support on the 1-cubed end-station. We thank HZB for the allocation of synchrotron radiation beamtime and thankfully acknowledge the financial support by HZB. This work was supported by CREST, Japan Science and Technology Agency, Grants-in-Aid for Scientific Research (Grants No. 16H02209, No. 25707030, and No. 26105002), by Grants-in-Aid for Scientific Research on Innovative Areas "J-Physics" (Grants No. 15H05882 and No. 15H05883) and Program for Advancing Strategic International Networks to Accelerate the Circulation of Talented Researchers (Grant No. R2604) from the Japanese Society for the Promotion of Science. A.H.N. was supported by Grant No. DMR-1350237 from the U.S. National Science Foundation.

[1] A. C. Hewson, *The Kondo Problem to Heavy Fermions* (Cambridge University Press, Cambridge, 1993).

[2] H. v. Löhneysen, A. Rosch, M. Vojta, and P. Wölfle, Rev. Mod. Phys. **79**, 1015 (2007).

[3] Y. Matsumoto, S. Nakatsuji, K. Kuga, Y. Karaki, N. Horie, Y. Shimura, T. Sakakibara, A. H. Nevidomskyy, and P. Coleman, Science **331**, 316 (2011).

[4] T. Tomita, K. Kuga, Y. Uwatoko, P. Coleman, and S. Nakatsuji, Science **349**, 506 (2015).

[5] Y. Matsumoto, K. Kuga, Y. Karaki, Y. Shimura, T. Sakakibara, M. Tokunaga, K. Kindo, and S. Nakatsuji, J. Phys. Soc. Jpn. **84**, 024710 (2015).

[6] S. Nakatsuji, K. Kuga, Y. Machida, T. Tayama, T. Sakakibara, Y. Karaki, H. Ishimoto, S. Yonezawa, Y. Maeno, E. Pearson, G. G. Lonzarich, L. Balicas, H. Lee, and Z. Fisk, Nat. Phys. **4**, 603 (2008).

[7] T. Misawa, Y. Yamaji, and M. Imada, J. Phys. Soc. Jpn. **78**, 084707 (2009).

[8] A. Ramires, P. Coleman, A. H. Nevidomskyy, and A. M. Tsvelik, Phys. Rev. Lett. **109**, 176404 (2012).

[9] J. H. Pixley, S. Kirchner, K. Ingersent, and Q. Si, Phys. Rev. Lett. **109**, 086403 (2012).

[10] A. Hackl and R. Thomale, Phys. Rev. B **83**, 235107 (2011).

[11] S. Watanabe and K. Miyake, J. Phys. Soc. Jpn. **83**, 103708 (2014).

[12] V. R. Shaginyan, A. Z. Msezane, K. G. Popov, J. W. Clark, V. A. Khodel, and M. V. Zverev, Phys. Rev. B **93**, 205126 (2016).

[13] E. C. T. O'Farrell, Y. Matsumoto, and S. Nakatsuji, Phys. Rev. Lett. **109**, 176405 (2012).

[14] Y. Matsumoto, K. Kuga, T. Tomita, Y. Karaki, and S. Nakatsuji, Phys. Rev. B **84**, 125126 (2011).

[15] R. T. Macaluso, S. Nakatsuji, K. Kuga, E. L. Thomas, Y. Machida, Y. Maeno, Z. Fisk, and J. Y. Chan, Chem. Mater. **19**, 1918 (2007).

[16] See Supplemental Material at http://link.aps.org/supplemental/10.1103/PhysRevB.97.045112 for a comparison, side by side, of laser-ARPES spectra of β-$YbAlB_4$ with linear polarized and circular polarized light, for examples of EDC fits performed in this work, for raw data of Figs. 2 and 4, and for details of hybridization models used in Figs. 2(c) and 2(d).

[17] P. Zhang, P. Richard, T. Qian, Y.-M. Xu, X. Dai, and H. Ding, Rev. Sci. Instrum. **82**, 043712 (2011).

[18] A. Damascelli, Phys. Scr. **T109**, 61 (2004).

[19] M. Okawa, M. Matsunami, K. Ishizaka, R. Eguchi, M. Taguchi, A. Chainani, Y. Takata, M. Yabashi, K. Tamasaku, Y. Nishino, T. Ishikawa, K. Kuga, N. Horie, S. Nakatsuji, and S. Shin, Phys. Rev. Lett. **104**, 247201 (2010).

[20] A. H. Nevidomskyy and P. Coleman, Phys. Rev. Lett. **102**, 077202 (2009).

[21] S.-K. Mo, W. S. Lee, F. Schmitt, Y. L. Chen, D. H. Lu, C. Capan, D. J. Kim, Z. Fisk, C.-Q. Zhang, Z. Hussain, and Z.-X. Shen, Phys. Rev. B **85**, 241103 (2012).

[22] E. C. T. O'Farrell, D. A. Tompsett, S. E. Sebastian, N. Harrison, C. Capan, L. Balicas, K. Kuga, A. Matsuo, K. Kindo, M. Tokunaga, S. Nakatsuji, G. Csányi, Z. Fisk, and M. L. Sutherland, Phys. Rev. Lett. **102**, 216402 (2009).

[23] N. W. Ashcroft and N. D. Mermin, *Solid State Physics* (Saunders College, Philadelphia, 1976).

[24] T. Senthil, S. Sachdev, and M. Vojta, Physica B **359-361**, 9 (2005).

[25] M. L. Sutherland, E. C. T. O'Farrell, W. H. Toews, J. Dunn, K. Kuga, S. Nakatsuji, Y. Machida, K. Izawa, and R. W. Hill, Phys. Rev. B **92**, 041114 (2015).

[26] A. Ramires and P. Coleman, Phys. Rev. Lett. **112**, 116405 (2014).

[27] L. M. Holanda, J. M. Vargas, W. Iwamoto, C. Rettori, S. Nakatsuji, K. Kuga, Z. Fisk, S. B. Oseroff, and P. G. Pagliuso, Phys. Rev. Lett. **107**, 026402 (2011).

[28] L. M. Holanda, G. G. Lesseux, E. T. Magnavita, R. A. Ribeiro, S. Nakatsuji, K. Kuga, Z. Fisk, S. B. Oseroff, R. R. Urbano, C. Rettori, and P. G. Pagliuso, J. Phys.: Condens. Matter **27**, 255601 (2015).